

Low Overhead Channel Estimation in MIMO OTFS Wireless Communication Systems

Kailong Wang , *Student Member, IEEE*, Athina Petropulu , *Fellow, IEEE*

Abstract—Orthogonal Time Frequency Space (OTFS) modulation has recently garnered attention due to its robustness in high-mobility wireless communication environments. In OTFS, the data symbols are mapped to the Doppler-Delay (DD) domain. In this paper, we address bandwidth-efficient estimation of channel state information (CSI) for MIMO OTFS systems. Existing channel estimation techniques either require non-overlapped DD-domain pilots and associated guard regions across multiple antennas, sacrificing significant communication rate as the number of transmit antennas increases, or sophisticated algorithms to handle overlapped pilots, escalating the cost and complexity of receivers. We introduce a novel pilot-aided channel estimation method that enjoys low overhead while achieving high performance. Our approach embeds pilots within each OTFS burst in the Time-Frequency (TF) domain. We propose a novel use of TF and DD guard bins, aiming to preserve waveform orthogonality on the pilot bins and DD data integrity, respectively. The receiver first obtains low-complexity coarse estimates of the channel parameters. Leveraging the orthogonality, a virtual array (VA) is constructed. This enables the formulation of a sparse signal recovery (SSR) problem, in which the coarse estimates are used to build a low-dimensional dictionary matrix. The SSR solution yields high-resolution estimates of channel parameters. Simulation results show that the proposed approach achieves good performance with only a small number of pilots and guard bins. Furthermore, the required overhead is independent of the number of transmit antennas, ensuring good scalability of the proposed method for large MIMO arrays. The proposed approach considers practical rectangular transmit pulse-shaping and receiver matched filtering, and also accounting for fractional Doppler effects.

Index Terms—Integrated Sensing and Communication, MIMO, OTFS, Channel Estimation, Embedded Pilots

I. INTRODUCTION

THE proliferation of high-mobility communication scenarios, such as vehicular-to-everything (V2X) and unmanned aerial vehicle (UAV) networks, has made achieving reliable, high-capacity, and low-latency wireless transmission a primary goal for 5G and beyond networks. A key challenge in these environments is the rapid time variation of the wireless channels [1]. Conventional orthogonal frequency-division multiplexing (OFDM) signaling [2], [3] degrades under such conditions due to the resulting Doppler effects. To mitigate these issues, the Orthogonal Time Frequency Space (OTFS) modulation scheme [4], [5] has emerged as a promising technology due to its inherent robustness against the Doppler shift

and its proven superior performance in fast fading channels. The fundamental difference of OTFS is its operation in the two-dimensional (2D) Doppler-delay (DD) domain, as opposed to the traditional time-frequency (TF) domain of OFDM. In this domain, the channel impulse response of a highly mobile environment is transformed into a sparse and quasi-time-invariant representation, which is characterized by a few key Doppler-delay parameters. This enables accurate equalization and signal detection in high-mobility scenarios.

To meet the ever-increasing demand for high throughput and spectral efficiency, OTFS can be integrated with Multiple-Input Multiple-Output (MIMO) [6] technology. MIMO systems enhance channel capacity and communication coverage by transmitting multiple data streams simultaneously and forming flexible beams, which also helps mitigate fading and interference. Beyond communication, MIMO has also proven important in radar systems [7], where its flexible beams, created by independent waveforms, allow for the simultaneous tracking of multiple targets. MIMO OTFS architecture can offer high-quality communication services even in extremely mobile scenarios. A prerequisite for fully realizing the high-capacity and spectral efficiency benefits of MIMO OTFS is the accurate estimation of Channel State Information (CSI).

Initial works on OTFS channel estimation primarily focused on SISO systems and adopted DD domain pilot-aided schemes. These schemes embed a pilot in the DD domain, surrounded by a zero guard region to prevent pilot-data interference [8]. While this design allows for the direct extraction of channel parameters at the receiver, the mandatory guard region constitutes signaling overhead, which limits the achievable communication rate. Building on this guard region design, [9], [10], [11], [12] achieve enhanced channel estimation and the capability to estimate fractional Doppler shifts by utilizing multiple embedded and mutually uncorrelated pilots within the DD domain. Later, using the same guard-region design, [13], [14], [15] showed that even a single pilot can be sufficient for fractional-Doppler and accurate CSI estimation when combined with more advanced algorithms, such as iterative estimation across the DD and time domains, deep learning, or sparse Bayesian learning. As a departure from DD domain pilots, [16] views the OTFS system as a precoded OFDM system, allowing low-complexity frequency-domain or time-domain pilot-aided channel estimation schemes to be applied. [16] uses a frequency-domain guard region for the frequency domain pilots, or a time-domain guard region for the time domain pilots, with approximately 50% reduced overhead as compared to the embedded DD pilots-guard region design.

Extending SISO embedded pilot-guard region schemes to

The work was supported by National Science Foundation (NSF) grant ECCS-2514270 and Army Research Office (ARO) grant W911NF2320103.

The authors are with the Department of Electrical and Computer Engineering, Rutgers University, Piscataway, NJ, 08854 USA (e-mail: kailong.wang@rutgers.edu; athinap@rutgers.edu).

MIMO systems is challenging. Among the aforementioned works, [8]–[15] have been extended to the MIMO case [17] by employing non-overlapping guard regions for each antenna. However, such guard regions significantly increase the overhead. MIMO methods utilizing embedded DD-domain pilots with overlapping guard regions across antennas have also been proposed, including [18], [19] for integer Doppler and [20], [21] for fractional Doppler. On each antenna, the pilots form a random complex Gaussian sequence. These sequences are independent across antennas, which ensures they remain separable at the receiver even when overlapped. Nevertheless, these methods still require large guard regions that must cover the maximum Doppler and delay spreads—parameters that are typically unknown—thereby resulting in substantial overhead.

There are also studies that eliminate the need for guard regions by superimposing pilots on data symbols. For SISO systems, both single [22], [23], [24] and full grid superimposed DD-domain pilots [25], [26] have been investigated, addressing integer and fractional Doppler shifts, respectively. Superimposed TF-domain pilots, placed at uniformly spaced subcarriers across all subsymbols, are considered in [27], allowing for the estimation of fractional Doppler. The aforementioned superimposed pilot approaches employ computationally complex self-interference-cancellation techniques to manage the overlap between pilots and data symbols, *i.e.*, iterative estimation of the channel and refinement of the estimate with coarsely recovered symbols until the effect of the data symbol is completely eliminated from the received pilot. The existing extension of the superimposed pilot-aided OTFS channel estimation to MIMO systems [28] relies on a block of OTFS symbols to estimate fractional Doppler and obtain accurate channel estimates, which may increase communication latency.

There are also channel estimation methods, where pilots are inserted between OTFS bursts. Both SISO channels [29], and MIMO channels [30], [31], [32], [33] have been considered. While this design avoids pilot-data interference, it does not provide the CSI corresponding to each OTFS burst.

In this paper, we propose a novel embedded-pilot-aided channel estimation method for MIMO OTFS systems. The proposed approach achieves channel estimation accuracy with significantly reduced overhead compared to existing methods, while effectively handling fractional Doppler. We model the wireless channel as a collection of discrete scatterers; thus, channel estimation is equivalent to estimating the scatterer parameters—angle of arrival (AoA), angle of departure (AoD), range, velocity, and reflection coefficient—using a bistatic radar model. One or more antennas introduce pilots in their TF domains within their OTFS burst. For each pilot, guard bins are created in both the TF and the DD domains. Here, the guard bins have different functions than in existing methods [8]–[21]. When antenna p introduces a pilot on TF bin $[n_p, m_p]$, TF guard bins containing zeros are entered at TF position $[n_p, m_p]$ of all other transmit antennas; in that way, the TF bin $[n_p, m_p]$ is private [34] to antenna p and waveform orthogonality holds on that bin at the receiver. For every pilot or guard bin created in the TF domain, one bin is left empty in the DD domain of the corresponding antenna, which is viewed as

a DD guard bin ensuring the integrity of the DD domain information. At the receiver, based on all TF bins, coarse estimates of AoA are obtained through a low-complexity operation. In that case, the AoA resolution is determined by the aperture of the receive array. Based on the signal received on the TF pilots, the obtained AoA estimates, and simple geometry, coarse estimates of the range, velocity, and AoD are obtained. The private TF pilots enforce orthogonality at the receiver, which can be exploited to construct a virtual array along with a discretization of the parameter space around the coarse estimates, providing high-resolution channel parameter estimates via sparse signal recovery (SSR) techniques. With this newly acquired CSI, equalization can then be performed. While our proposed pilots and guard bins represent overhead, only a small number of them is sufficient to achieve high-quality channel estimates with minimal communication rate loss.

The novelty of our contribution is summarized as follows.

- A novel pilot placement scheme in the TF domain is proposed, enabling channel estimation with significantly reduced overhead compared to prior methods. Pilots are inserted into selected TF-domain bins, accompanied by guard bins in both the TF and DD domains. Only a small number of pilots and guard bins are required to achieve high performance, thereby incurring minimal overhead.
- The TF pilots are placed along P_τ consecutive bins parallel to the frequency axis, and along P_ν consecutive bins parallel to the time axis, with one common bin; the total number of pilots is $N_p \approx P_\tau + P_\nu$. The values of P_τ and P_ν determine the resolution of the coarse range and velocity estimates. Even small values can significantly reduce the parameter space that must be discretized for constructing the SSR problem, thereby lowering the complexity of obtaining high-resolution channel estimates.
- For a total number of N_p TF domain pilots, $N_p(N_t - 1)$ TF domain guard bins, and $N_t N_p$ DD domain guard bins are required. The corresponding reduction of $N_t N_p$ DD domain symbols represents the overall overhead, *i.e.*, $\eta = N_t N_p / (N_t N M) = N_p / (N M)$. The overhead is independent of the number of transmit antennas, offering superior scalability for large MIMO arrays—a desirable feature for future wireless systems.
- The proposed channel estimation is applicable to practical OTFS systems, considering rectangular transmitter pulse-shaping functions and the receiver matched filters.

Relation to the literature. The proposed CSI estimation method is inspired by our recent work on dual-function radar communication (DFRC) MIMO OTFS radar systems [34], [35], [36], where sensing with a colocated MIMO receiver was considered, and the concept of TF private bins was introduced to construct a virtual array. In [34], [35], [36], the estimation of the targets can be viewed as the estimation of the sensing channel, implemented by a colocated receiver based on knowledge of the transmitted symbols. In this proposed paper, CSI estimation can be viewed as the estimation of the sensing channel by a well-separated communication receiver, and is implemented based on knowledge of the transmitted pilots. In

our preliminary work [37], we explored channel estimation using pilots placed on TF private bins. However, we assumed that the transmitter's channel estimates could be conveyed to the receiver along with the information-bearing symbols. This implies that the receiver relies on potentially outdated CSI for equalization. In fast-varying channels, however, accurate receiver-side channel estimation becomes essential. Furthermore, unlike [37], this work considers practical rectangular transmit pulse shaping and receiver matched filtering, while also accounting for fractional Doppler effects.

Paper organization. The paper is organized as follows. In Section II, we briefly describe the MIMO OTFS modulation and demodulation process, along with the channel model. In Section III, we introduce our TF pilots and guard bins design in both the TF and DD domains, and present the corresponding pilot placement pattern. In Section IV, we propose a low-complexity algorithm for obtaining coarse estimates of the channel parameters. In Section V, we describe the construction of a virtual array and show how it can be used, along with a discretized channel parameter space centered around the coarse estimates, to refine the channel estimates via the SSR technique. In Section VI, we extend the design to the fractional Doppler case. The recovery of transmitted symbols is discussed in Section VII. We analyze the overhead and computational complexity of our design by comparing it with existing methods in Section VIII. Finally, we demonstrate the performance of the proposed system through simulations in Section IX, and conclude the paper in Section X.

II. MIMO-OTFS SYSTEM MODEL

We consider a wireless system comprising a transmitter with N_t antennas (TX) and a communication receiver with N_c antennas. The transmit waveforms are OTFS, carrier frequency is f_c Hz, and the wavelength is $\lambda = c/f_c$ with c being the speed of light. The transmit and receive antennas form uniform linear arrays (ULA) with spacing g_t and g_c , respectively.

The transmit antennas simultaneously transmit packet bursts of duration $T = N\Delta t$ and bandwidth $B = M\Delta f$, where N is the number of subsymbols, M is the number of subcarriers, Δt is the subsymbol duration, and Δf is the subcarrier spacing. The orthogonality condition requires that $\Delta t \cdot \Delta f = 1$ [5]. In each burst, a set of NM symbols is arranged on the DD grid,

$$\{ [k\Delta\nu, l\Delta\tau] \mid k = 0, 1, \dots, N-1; l = 0, 1, \dots, M-1 \},$$

where k and l are Doppler and delay indices. The grid spacing is $\Delta\nu = 1/(N\Delta t)$ and $\Delta\tau = 1/(M\Delta f)$.

We employ the angular DD domain channel model [30], consisting of J scatterers at AoA θ_j and AoD φ_j , *i.e.*,

$$\mathbf{h}(\theta, \varphi, \tau, \nu) = \sum_{j=0}^{J-1} \beta_j \mathbf{a}_c(\theta_j) \mathbf{a}_t^H(\varphi_j) \delta(\tau - \tau_j) \delta(\nu - \nu_j), \quad (1)$$

where β_j is the complex channel attenuation factor, $\mathbf{a}_c(\theta_j)$ is the AoA steering vector, $\mathbf{a}_t(\varphi_j)$ is the AoD steering vector, τ_j is the delay corresponding to range R_j ($\tau_j = R_j/c$), and ν_j is the Doppler corresponding to radial velocity v_j sensed by the receiver ($\nu_j = v_j/\lambda$) of the j -th scatterer, respectively. Each

scatterer's Doppler and delay do not necessarily align with the DD grid. A typical assumption is that the j -th scatterer's Doppler and delay can be expressed as

$$\nu_j = (k_j + \kappa_j)\Delta\nu, \quad \tau_j = l_j\Delta\tau, \quad (2)$$

where k_j, l_j are integers and $\kappa_j \in [-1/2, 1/2]$ denotes fractional Doppler. The impact of fractional delays in wideband systems can be neglected [5] since the delay spacing $\Delta\tau$ is typically sufficiently small. The dimensions of the grid should satisfy $N \geq 2\max|k_j| + 1$ and $M \geq \max l_j$ so that it can support all present Doppler and delays. In high-frequency scenarios, which will arise in next-generation communications, the DD channel is sparse, *i.e.*, it contains a small number of paths. For ease of presentation, in this section we present the idea of integer Doppler, *i.e.*, $\kappa_j = 0$, and later in Section VI we consider the fractional case.

Let $x_{n_t}[k, l]$ be the symbol of the n_t -th antenna placed on DD bin $[k, l]$. The symbols are mapped to the TF domain via the Inverse Symplectic Finite Fourier Transform (ISFFT) [5],

$$X_{n_t}[n, m] = \frac{1}{NM} \sum_{k=0}^{N-1} \sum_{l=0}^{M-1} x_{n_t}[k, l] e^{i2\pi(\frac{kn}{N} - \frac{ml}{M})}. \quad (3)$$

The analog signal for transmission, $s_{n_t}(t)$, is created via the Heisenberg Transform [5], *i.e.*,

$$s_{n_t}(t) = \sum_{n=0}^{N-1} \sum_{m=0}^{M-1} X_{n_t}[n, m] g_{tx}(t - n\Delta t) e^{i2\pi m\Delta f(t - n\Delta t)}, \quad (4)$$

where $g_{tx}(t)$ is the pulse function, taken here to be a rectangular pulse with amplitude $1/\sqrt{\Delta t}$ for $t \in [0, \Delta t]$ and 0 at all other times. We also assume that a cyclic prefix (CP) of length greater than $\max l_j$ is appended to $s_{n_t}(t)$ before transmission, so that the interference between OTFS symbols is avoided.

The noiseless received signal at the n_c -th receive antenna is

$$r_{n_c}(t) = \sum_{j=0}^{J-1} e^{-i2\pi n_c g_c \frac{\sin(\theta_j)}{\lambda}} \sum_{n_t=0}^{N_t-1} e^{-i2\pi n_t g_t \frac{\sin(\varphi_j)}{\lambda}} \times s_{n_t}(t - \tau_j) \beta_j e^{i2\pi \nu_j(t - \tau_j)}. \quad (5)$$

After matched filtering with matched filter $g_{cx}(t) = g_{tx}(t)$, and sampling over a duration T at frequency B , the received TF domain signal $Y_{n_c}[n, m]$ is obtained. On performing an SFFT on $Y_{n_c}[n, m]$, the demodulated symbol at DD bin $[k, l]$ can be obtained as [5]

$$\begin{aligned} y_{n_c}[k, l] &= \sum_{n=0}^{N-1} \sum_{m=0}^{M-1} Y_{n_c}[n, m] e^{-i2\pi(\frac{kn}{N} - \frac{ml}{M})} \\ &= \sum_{j=0}^{J-1} e^{-i2\pi n_c g_c \frac{\sin(\theta_j)}{\lambda}} \sum_{n_t=0}^{N_t-1} e^{-i2\pi n_t g_t \frac{\sin(\varphi_j)}{\lambda}} \alpha_j[k, l] \\ &\quad \times x_{n_t}[[k - k_j]_N, [l - l_j]_M] \beta_j e^{-i2\pi \frac{k_j l_j}{NM}}, \end{aligned} \quad (6)$$

where

$$\alpha_j[k, l] = \begin{cases} e^{i2\pi \frac{k_j l_j}{NM}} & l_j \leq l < M, \\ \frac{N-1}{N} e^{i2\pi \frac{k_j l_j}{NM}} e^{-i2\pi \frac{[k-k_j]_N}{N}} & 0 \leq l < l_j. \end{cases} \quad (8)$$

Based on Eq. (7), the vectorized MIMO-OTFS channel input-output relation can be expressed as

$$\mathbf{y}_{\text{MIMO}} = \mathbf{h}_{\text{MIMO}} \mathbf{x}_{\text{MIMO}}, \quad (9)$$

where $\mathbf{y}_{\text{MIMO}} \in \mathbb{C}^{N_c N M}$, $\mathbf{x}_{\text{MIMO}} \in \mathbb{C}^{N_t N M}$ are respectively the received and transmitted DD domain symbols of all antennas, with the symbols of each antenna taken in a row-wise fashion; $\mathbf{h}_{\text{MIMO}} \in \mathbb{C}^{N_c N M \times N_t N M}$ is a sparse matrix whose $l + kM + n_c N M$ -th row has non-zero entries on the $[l - l_j]_M + [k - k_j]_N M + n_t N M$ -th column, equal to

$$e^{-i2\pi n_c g_c \frac{\sin(\theta_j)}{\lambda}} e^{-i2\pi n_t g_t \frac{\sin(\varphi_j)}{\lambda}} \alpha_j[k, l] \beta_j e^{-i2\pi \frac{k_j l_j}{N M}}, \quad (10)$$

for all $n_c \in [0, 1, \dots, N_c - 1]$, $n_t \in [0, 1, \dots, N_t - 1]$ and $j \in [0, 1, \dots, J - 1]$. We can express \mathbf{h}_{MIMO} as [30]

$$\mathbf{h}_{\text{MIMO}} = \sum_{j=0}^{J-1} \beta_j (\mathbf{a}_c(\theta_j) \mathbf{a}_t^H(\varphi_j)) \otimes (\mathbf{F}_N \otimes \mathbf{I}_M) (\Pi^{\frac{\tau_j}{\Delta \tau}} \Delta^{\frac{\nu_j}{\Delta \nu}}) (\mathbf{F}_N^H \otimes \mathbf{I}_M), \quad (11)$$

where \otimes is the Kronecker product, \mathbf{F}_N is the DFT matrix of order N , \mathbf{I}_M is the identity matrix of order M , Π is the forward cyclic shift permutation matrix of size $N M \times N M$, and $\Delta = \text{diag}[z^0, z^1, \dots, z^{N M - 1}]$ with $z = e^{i2\pi \frac{1}{N M}}$.

Knowing the channel (*i.e.*, the parameters of the channel scatterers), the transmitted symbols can be obtained via LMMSE equalization.

III. TF-DOMAIN PILOTS GUARDED BY TF AND DD-DOMAIN BINS

We propose placing pilots in a certain configuration on private TF bins. Let us recall the concept of private bins introduced in [34]. Private bin $[n_p, m_p]$ for transmit antenna p is created by enforcing zeros in bin $[n_p, m_p]$ of all other transmit antennas. The zero bins can be viewed as TF guard bins, preserving the private usage of bin $[n_p, m_p]$ for the transmit antenna p . Since each TF bin contains a linear combination of all DD-domain symbols through the ISFFT, enforcing a zero or inserting a pilot in the TF domain reduces by one the number of available equations for recovering DD information from TF observations. This effect can be mitigated by reducing the number of DD symbols by one through the introduction of an empty bin in the DD domain prior to applying the ISFFT. The empty bins can be viewed as DD guard bins, preserving the integrity of the DD domain information. An example, consider a $N_t = 2$, $N = M = 4$ system, is illustrated in Fig. 1. A pilot symbol is placed in the TF bin $[0, 0]$ of antenna TX_1 . Simultaneously, the TF bin $[0, 0]$ of TX_2 is set to zero and serves as a TF guard bin, ensuring that the $[0, 0]$ bin is used exclusively by TX_1 . To prevent the pilot and zero TF bins from disturbing the DD-domain information, one bin in each antenna's DD domain must have been left empty. Therefore, although one TF bin is reserved for the pilot (or set to zero), the remaining 15 TF bins provide 15 linear equations in the DD-domain symbols, and thus, no DD information is lost.

We propose a pilot pattern as illustrated in Fig. 2 for the $N_t = 2$ case. A total of $N_p = P_\tau + P_\nu - 1$ pilots are placed

on antenna 1; the pilot pattern is anchored at $[n_{p_0}, m_{p_0}]$ with $p = 1$, and spans P_τ bins along the frequency axis, to be referred to as the *frequency arm*, and P_ν bins along the time axis, to be referred to as the *time arm*. Although Figs. 1 and 2 uses 1 to denote pilots, the pilots are random i.i.d.

The set $\mathcal{P}_p(n_{p_0}, m_{p_0}; P_\tau, P_\nu)$, $p = 0, 1, \dots, N_t - 1$ is used to denote the pilot support of antenna p . The pilot power is scaled to match the average power of the transmitted symbols, thus ensuring a uniform transmission power level.

The location of the TF pilot/guard bins needs to be conveyed to the communication receiver. This information can be passed by transmitting the quantities $\mathcal{P}_p(n_{p_0}, m_{p_0}; P_\tau, P_\nu)$, $p = 0, 1, \dots, N_t - 1$. The location of the DD guard bins and the value of pilots also need to be communicated to the receiver.

IV. LOW COMPLEXITY COARSE CHANNEL ESTIMATION

The channel constitutes a collection of J scatterers, each with complex attenuation factor β_j , and parameters $(\theta_j, \varphi_j, \tau_j, \nu_j)$, where θ_j is the AoA, φ_j is the AoD, τ_j is the delay, ν_j is the Doppler for the j -th scatterer, respectively. Channel estimation breaks down to estimating these parameters. In the following, we demonstrate how to obtain coarse estimates of these parameters using a low-complexity approach that utilizes the proposed pilot pattern.

Coarse estimation of θ_j : On expressing $x_{n_t}[[k - k_j]_N, [l - l_j]_M]$ as the SFFT of $X_{n_t}[n', m']$ and substituting into the ISFFT of Eq. (7), we get

$$Y_{n_c}[n, m] = \sum_{n_t=0}^{N_t-1} X_{n_t}[n, m] \sum_{j=0}^{J-1} e^{-i2\pi n_c g_c \frac{\sin(\theta_j)}{\lambda}} e^{-i2\pi n_t g_t \frac{\sin(\varphi_j)}{\lambda}} \xi_j \beta_j e^{-i2\pi \frac{k_j l_j}{N M}} e^{i2\pi \left(\frac{k_j n}{N} - \frac{m l_j}{M} \right)} + I_{n_c}[n, m], \quad (12)$$

where

$$\xi_j = \frac{1}{N M} \sum_{k=0}^{N-1} \sum_{l=0}^{M-1} \alpha_j[k, l] = \frac{1}{M} \frac{e^{i2\pi \frac{k_j l_j}{N M}} - e^{i2\pi \frac{k_j}{N}}}{1 - e^{i2\pi \frac{k_j}{N M}}} \quad (13)$$

and $I_{n_c}[n, m]$, denoting interference, is equal to

$$I_{n_c}[n, m] = \sum_{n_t=0}^{N_t-1} \sum_{n' \neq n, n'=0}^{N-1} \sum_{m' \neq m, m'=0}^{M-1} X_{n_t}[n', m'] \times \sum_{j=0}^{J-1} e^{-i2\pi n_c g_c \frac{\sin(\theta_j)}{\lambda}} e^{-i2\pi n_t g_t \frac{\sin(\varphi_j)}{\lambda}} \frac{1}{N M} \sum_{k=0}^{N-1} \sum_{l=0}^{M-1} \alpha_j[k, l] \times \beta_j e^{-i2\pi \frac{k_j l_j}{N M}} e^{-i2\pi \left(\frac{k(n' - n) - k_j n'}{N} - \frac{(m' - m)l - m' l_j}{M} \right)}. \quad (14)$$

Since TF symbols $X_{n_t}[n', m']$ are random with zero mean, the term $I_{n_c}[n, m]$ can be modeled as additive zero-mean noise.

In the following, the interference term $I_{n_c}[n, m]$ and also the additive noise are neglected for analytical tractability. Their impact on the estimation results will become evident in Section IX. Ignoring $I_{n_c}[n, m]$, we can rewrite Eq. (12) as

$$Y_{n_c}[n, m] = \sum_{j=0}^{J-1} A_j[n, m] e^{-i2\pi n_c g_c \frac{\sin(\theta_j)}{\lambda}}, \quad (15)$$

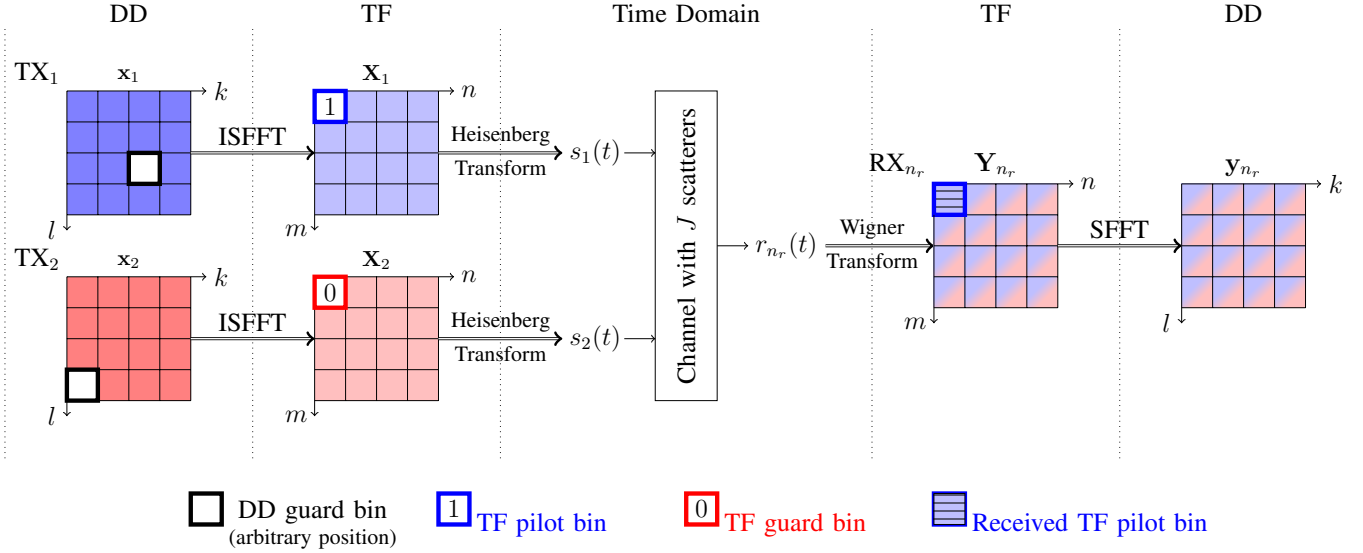


Fig. 1. Pilot and guard bins in the TF and DD domains. TF guard bins maintain orthogonality. DD guard bins preserve the integrity of information symbols.

where

$$A_j[n, m] = \sum_{n_t=0}^{N_t-1} X_{n_t}[n, m] e^{-i2\pi n_t g_t \frac{\sin(\varphi_j)}{\lambda}} \xi_j \beta_j H^j[n, m], \quad (16)$$

$$H^j[n, m] = e^{-i2\pi \frac{k_j l_j}{NM}} e^{i2\pi \left(\frac{k_j n}{N} - \frac{m l_j}{M} \right)}. \quad (17)$$

Based on Eq. (15), $Y_{n_c}[n, m]$, viewed as a function of n_c , for $n_c = 0, 1, \dots, N_c - 1$, is the sum of J discrete time complex sinusoids, each with frequency $g_c \sin(\theta_j)/\lambda$ and corresponding complex amplitude $A_j[n, m]$. The frequencies and corresponding amplitudes can be found, among various spectrum estimation methods, using an N_c -point DFT. Based on the frequencies, the AoAs $\hat{\theta}_j$, serving as coarse estimates of θ_j , can then be determined. The DFT-based estimation can be applied to all TF-domain bins $[n, m]$, and the resulting angle estimates can then be averaged.

The resolution of $\hat{\theta}_j$ depends on the aperture of the receive array. The DFT peaks may not align with the ground truth.

Coarse estimation of τ_j, ν_j : After the $\hat{\theta}_j$ s have been estimated, the $A_j[n, m]$ s can be obtained from Eq. (15) in the LS sense. The complex amplitude corresponding to $\hat{\theta}_j$ at pilot

bins $[n_p, m_p]$ divided by the known pilots, can be expressed as (see Eq. (16))

$$\frac{A_j[n_p, m_p]}{X_p[n_p, m_p]} = e^{-i2\pi p g_t \frac{\sin(\varphi_j)}{\lambda}} \xi_j \beta_j H^j[n_p, m_p]. \quad (18)$$

Note, due to the private nature of pilot bins, the summation over N_t reduces to a single term corresponding to antenna p .

Consider the ratio of Eq. (18) on center pilots over Eq. (18) on frequency arm pilots of antenna p , i.e.,

$$R_p(m_{p_0}, m_{p_1}; n_{p_0}) \triangleq \frac{A_j[n_{p_0}, m_{p_0}]}{X_p[n_{p_0}, m_{p_0}]} \frac{X_p[n_{p_0}, m_{p_1}]}{A_j[n_{p_0}, m_{p_1}]} \quad (19)$$

$$= e^{i2\pi l_j (m_{p_1} - m_{p_0})/M}, \quad (20)$$

where $[n_{p_0}, m_{p_1}] \in \mathcal{P}_p(n_{p_0}, m_{p_0}; P_\tau, P_\nu)$. By setting $m_{p_1} = m_{p_0} + \ell$, $\ell = 0, 1, \dots, P_\tau - 1$, Eq. (20) becomes

$$R_p(m_{p_0}, m_{p_0} + \ell; n_{p_0}) = e^{i2\pi \frac{l_j}{M} \ell}, \quad (21)$$

for $\ell = 0, 1, \dots, P_\tau - 1$, which is the sum of N_j complex sinusoids with discrete frequency l_j/M . Assuming that $P_\tau > N_j$ and taking an IDFT of length P_τ of the sequence $\{R(m_{p_0}, m_{p_0} + \ell; n_{p_0}) \mid \ell = 0, 1, \dots, P_\tau - 1\}$, the position of peaks will reveal the coarse estimates $\hat{\tau}_j$.

It also holds that (for the Eq. (18) on time arm of antenna q)

$$V_q(n_{q_0}, n_{q_1}; m_{q_0}) \triangleq \frac{A_j[n_{q_0}, m_{q_0}]}{X_q[n_{q_0}, m_{q_0}]} \frac{X_q[n_{q_1}, m_{q_0}]}{A_j[n_{q_1}, m_{q_0}]} \quad (22)$$

$$= e^{-i2\pi k_j (n_{q_1} - n_{q_0})/N}, \quad (23)$$

where $[n_{q_1}, m_{q_0}] \in \mathcal{P}_q(n_{q_0}, m_{q_0}; P_\tau, P_\nu)$. Similarly, the coarse estimates $\hat{\nu}_j$ can be obtained based on an P_ν -DFT of the sequence $\{V(n_{q_0}, n_{q_0} + \nu; m_{q_0}) \mid \nu = 0, 1, \dots, P_\nu - 1\}$.

In general, the time and frequency arms can be placed on different antennas ($p \neq q$). For illustration purposes, in Fig. 2 they are placed on the same antenna ($p = q$). In all cases, for each p , zeros (TF guard bins) are placed in bins

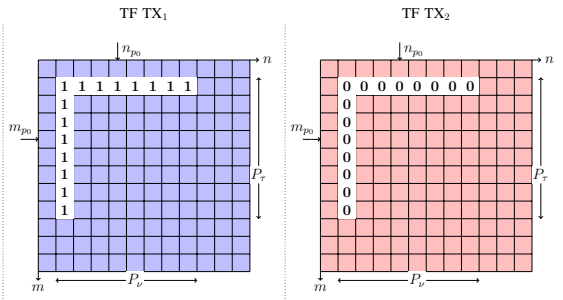


Fig. 2. TF domain pilots (indicated by '1's) on TX₁, and TF guard bins (indicated by '0's) on TX₂. Each antenna has 15 empty bins in the DD domain.

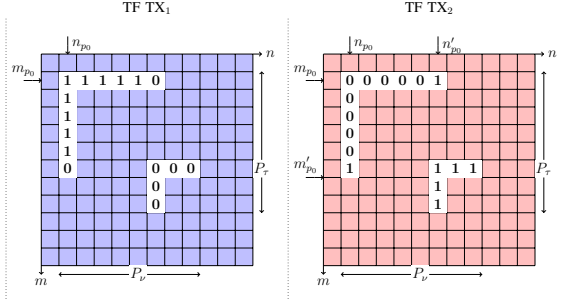


Fig. 3. Different parts of the frequency and time arms on different antennas.

$\mathcal{P}_r(n_{p_0}, m_{p_0}; P_\tau, P_\nu)$ for all $r \neq p$ to maintain the privacy of the pilot bins of antenna p .

We can also distribute parts of the frequency and time arms on several antennas, to benefit from diversity. For example, we can consider spreading the frequency arm of the pilots in two antennas, and estimate l_j based on $[\{R_1(m_0, m_0 + \ell; n_0) \mid \ell = 0, \dots, P_\tau/2 - 1\}, \{R_2(m_0, m_0 + \ell; n'_0) \mid \ell = P_\tau/2, \dots, P_\tau - 1\}]$. More parts are also valid. Every part needs one anchor point, increasing N_p when multiple parts are considered. It is possible that two parts result in one cross point, reducing N_p when multiple cross points exist. Thus, the total number of pilots is $N_p \approx P_\tau + P_\nu$. The above idea is illustrated in Fig. 3.

The resolution of $\hat{\tau}_j$ depends on P_τ , and the resolution of $\hat{\nu}_j$ depends on P_ν . The maximum possible resolution is achieved when $P_\tau = M$ and $P_\nu = N$. It is possible that, due to low resolution, the DFT peaks may not align with the ground truth. *Remark* - Eqs. (20) and (23), evaluated at different pilots, provide equations which can be used to solve for k_j, l_j . We chose the particular arrangement of pilots described above because it enables us to use a DFT for the estimation. Furthermore, it does not require a large overhead to convey the location of the pilots to the receiver.

Coarse estimation of φ_j : After coarse estimates of AoAs, $\hat{\theta}_j$, and delays, $\hat{\tau}_j$ have been obtained, coarse estimates of AoDs $\hat{\varphi}_j$ can be derived using the law of cosines. Based on Fig. 4, for the range estimates it holds that $c\hat{\tau}_j = \hat{R}_j = \hat{R}_{cj} + \hat{R}_{jt}$. The LoS distance, R_{LoS} , is either known beforehand (for fixed base stations) or it is calculated by the signal's travel time, τ_{LoS} , i.e., $R_{\text{LoS}} = c\tau_{\text{LoS}}$. Based on the law of cosines, we get

$$(\hat{R}_j - \hat{R}_{cj})^2 = \hat{R}_{jt}^2 = R_{\text{LoS}}^2 + \hat{R}_{cj}^2 - 2R_{\text{LoS}}\hat{R}_{cj} \cos(\hat{\theta}_j), \quad (24)$$

based on which, it holds that

$$\hat{R}_{cj} = \frac{\hat{R}_j^2 - R_{\text{LoS}}^2}{2(\hat{R}_j - R_{\text{LoS}} \cos(\hat{\theta}_j))}. \quad (25)$$

Applying the law of cosines again, we get that

$$\hat{R}_{cj}^2 = R_{\text{LoS}}^2 + \hat{R}_{jt}^2 - 2R_{\text{LoS}}\hat{R}_{jt} \cos(\hat{\varphi}_j), \quad (26)$$

based on which, it holds that

$$\hat{\varphi}_j = \arccos \frac{R_{\text{LoS}}^2 + \hat{R}_{jt}^2 - \hat{R}_{cj}^2}{2R_{\text{LoS}}\hat{R}_{jt}}. \quad (27)$$

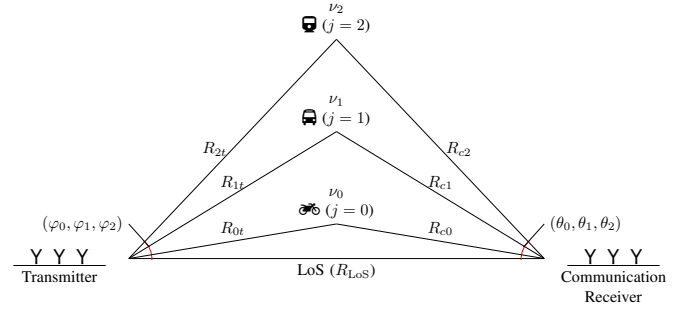


Fig. 4. Bi-static radar geometry model with 3 scatterers.

The resolution of the $\hat{\varphi}_j$ depends on coarse estimates $\hat{\theta}_j$ and \hat{R}_j . Hence, it is coarse as well.

After acquiring the coarse estimates, $(\hat{\theta}_j, \hat{\varphi}_j, \hat{\tau}_j, \hat{\nu}_j)$, the coarse channel attenuation factor $\hat{\beta}_j$ can be obtained by the pilots on all receive antennas in the LS sense. However, the resolution of those estimates is limited by the number of receive antennas and the number of pilots, resulting in estimation errors that lead to poor symbol detection performance. In Section V, we show how to improve on those low-resolution estimates by constructing a virtual array.

V. VIRTUAL ARRAY AND SPARSE SIGNAL RECOVERY

Based on the received signal on bin $[n_p, m_p]$, and knowledge of the corresponding pilots, $X_p[n_p, m_p]$, each receive antenna forms the ratio $Y_{n_c}[n_p, m_p]/X_p[n_p, m_p]$. These ratios are then collected into the vector $\mathbf{r}_p \in \mathbb{C}^{N_c \times 1}$, which is expressed as

$$\mathbf{r}_p = \mathbf{\Phi}_p(\theta_j, \varphi_j, \tau_j, \nu_j; n_p, m_p)\boldsymbol{\beta}, \quad (28)$$

where $\mathbf{\Phi}_p \in \mathbb{C}^{N_c \times J}$ is a matrix whose (n_c, j) -th element is

$$e^{-i2\pi n_c g_c \frac{\sin(\theta_j)}{\lambda}} e^{-i2\pi p g_t \frac{\sin(\varphi_j)}{\lambda}} \xi_j H^j[n_p, m_p], \quad (29)$$

and $\boldsymbol{\beta} = [\beta_0, \beta_1, \dots, \beta_{J-1}]^\top$.

By stacking the vectors corresponding to all pilot bins, i.e., $\{\mathbf{r}_p \mid p = 0, 1, \dots, N_p - 1\}$, in vector $\mathbf{r} \in \mathbb{C}^{N_c N_p \times 1}$, the receiver formulates the problem

$$\mathbf{r} = \mathbf{\Phi}\boldsymbol{\beta}, \quad (30)$$

where each column of $\mathbf{\Phi} \in \mathbb{C}^{N_c N_p \times J}$ is characterized by parameters $(\theta_j, \varphi_j, \tau_j, \nu_j)$ corresponding to the j -th scatterer. Eq. (30) provides a virtual array, which can enable N_p -fold improvement of the sensing resolution achievable by the physical receive array.

Vector \mathbf{r} can also be expressed in terms of an overcomplete matrix $\tilde{\mathbf{\Phi}}$, formed by discretizing the parameter space of $(\theta_j, \varphi_j, \tau_j, \nu_j)$, where $\theta_j \in [-\frac{\pi}{2}, \frac{\pi}{2}]$, $\varphi_j \in [-\frac{\pi}{2}, \frac{\pi}{2}]$, $\tau_j \in [0, \tau_{\text{max}}]$, $\nu_j \in [-\frac{\nu_{\text{max}}}{2}, \frac{\nu_{\text{max}}}{2}]$, where $\tau_{\text{max}} = 1/\Delta f$ is the maximum unambiguous delay and $\nu_{\text{max}} = 1/\Delta t$ is the maximum unambiguous Doppler.

Discretizing the entire space would lead to an unmanageable $\tilde{\mathbf{\Phi}}$. However, given the already obtained coarse estimates, we can make the problem more manageable. We can constrain the parameter space around coarse estimates, i.e., $\tilde{\theta}_j \in [\hat{\theta}_j -$

$\frac{\pi}{2N_c}, \hat{\theta}_j \in [\hat{\varphi}_j - \frac{\pi}{2N_c}, \hat{\varphi}_j + \frac{\pi}{2N_c}]$, $\tilde{\varphi}_j \in [\hat{\varphi}_j - \frac{\pi}{2N_c}, \hat{\varphi}_j + \frac{\pi}{2N_c}]$, $\tilde{\tau}_j \in [\hat{\tau}_j - \frac{\tau_{\max}}{2P_\tau}, \hat{\tau}_j + \frac{\tau_{\max}}{2P_\tau}]$, $\tilde{\nu}_j \in [\hat{\nu}_j - \frac{\nu_{\max}}{4P_\nu}, \hat{\nu}_j + \frac{\nu_{\max}}{4P_\nu}]$, obtaining $G_\theta, G_\varphi, G_\tau, G_\nu$ grid points, each corresponding to $(\tilde{\theta}_j, \tilde{\varphi}_j, \tilde{\tau}_j, \tilde{\nu}_j)$.

Eq. (30) becomes

$$\mathbf{r} = \tilde{\Phi} \tilde{\beta}, \quad (31)$$

where $\tilde{\Phi} \in \mathbb{C}^{N_c N_p \times G_\theta G_\varphi G_\tau G_\nu}$ has elements like Φ with parameters replaced by the discretized points; $\tilde{\beta} \in \mathbb{C}^{G_\theta G_\varphi G_\tau G_\nu \times 1}$ is a sparse vector, whose J non-zero entries correspond to grid points in the scatterer parameters' space. Then, $\tilde{\beta}$ can be obtained by solving a sparse signal recovery (SSR) problem via orthogonal matching pursuit (OMP) [38], *i.e.*,

$$\begin{aligned} \min \quad & \|\tilde{\beta}\|_0, \\ \text{S.T.} \quad & \|\mathbf{r} - \tilde{\Phi} \tilde{\beta}\|_2 \leq \epsilon. \end{aligned} \quad (32)$$

OMP is an iterative process that stops when the residual is less than ϵ , in which case, further iterations capture noise instead of the scatterers' parameters. Finally, the location of the non-zero entries of $\tilde{\beta}$ provides estimates of $(\theta_j, \varphi_j, \tau_j, \nu_j)$ and the actual values provide estimates of β_j for all $j = 0, 1, \dots, J-1$. Substituting these refined estimates into Eq. (11) provides an accurate CSI for the symbol detection.

VI. FRACTIONAL DOPPLER

The above analysis can be extended to fractional Doppler, *i.e.*, $\kappa_j \neq 0$ (see Eq. (2)). In that case, Eq. (7) becomes [5]

$$\begin{aligned} y'_{n_c}[k, l] = & \sum_{j=0}^{J-1} e^{-i2\pi n_c g_c \frac{\sin(\theta_j)}{\lambda}} \sum_{n_t=0}^{N_t-1} e^{-i2\pi n_t g_t \frac{\sin(\varphi_j)}{\lambda}} \sum_{q=-N_j}^{N_j} \\ & \times \alpha'_j[k, l, q] x_{n_t}[[k - (k_j - q)]_N, [l - l_j]_M] \beta_j e^{-i2\pi \frac{(k_j + \kappa_j) l_j}{NM}}, \end{aligned} \quad (33)$$

where $\alpha'_j[k, l, q]$ is

$$\begin{cases} \frac{1}{N} \gamma_j(q) e^{i2\pi \frac{(k_j + \kappa_j) l}{NM}}, & l_j \leq l < M, \\ \frac{1}{N} (\gamma_j(q) - 1) e^{i2\pi \frac{(k_j + \kappa_j) l}{NM}} e^{-i2\pi \frac{[k - (k_j - q)]_N}{N}}, & 0 \leq l < l_j, \end{cases} \quad (34)$$

with $\gamma_j(q) = \frac{e^{-i2\pi(-q - \kappa_j)} - 1}{e^{-i2\pi(-q - \kappa_j)/N} - 1} \neq N$ due to the non-zero fractional term κ_j .

Along the lines of Section III, the TF signal of communication receive antenna n_c corresponding to private bin $[n_p, m_p]$ of transmit antenna p equals

$$\begin{aligned} Y'_{n_c}[n_p, m_p] = & \sum_{j=0}^{J-1} e^{-i2\pi n_c g_c \frac{\sin(\theta_j)}{\lambda}} e^{-i2\pi p g_t \frac{\sin(\varphi_j)}{\lambda}} \xi'_j[n_p] \\ & \times X_p[n_p, m_p] \beta_j e^{-i2\pi \frac{(k_j + \kappa_j) l_j}{NM}} e^{i2\pi \left(\frac{k_j n_p}{N} - \frac{m_p l_j}{M} \right)} + I'_{n_c}[n_p, m_p], \end{aligned} \quad (35)$$

where

$$\xi'_j[n_p] = \frac{1}{NM} \sum_{k=0}^{N-1} \sum_{l=0}^{M-1} \sum_{q=-N_j}^{N_j} \alpha'_j[k, l, q] e^{-i2\pi \frac{q n_p}{N}} \quad (36)$$

$$= \frac{1}{NM} \sum_{l=l_j}^{M-1} e^{i2\pi \frac{(k_j + \kappa_j) l}{NM}} \sum_{q=-N_j}^{N_j} \gamma_j(q) e^{-i2\pi \frac{q n_p}{N}}, \quad (37)$$

and

$$\begin{aligned} I'_{n_c}[n_p, m_p] = & \sum_{j=0}^{J-1} e^{-i2\pi n_c g_c \frac{\sin(\theta_j)}{\lambda}} e^{-i2\pi p g_t \frac{\sin(\varphi_j)}{\lambda}} \\ & \times \frac{1}{NM} \sum_{k=0}^{N-1} \sum_{l=0}^{M-1} \sum_{q=-N_j}^{N_j} \alpha'_j[k, l, q] \sum_{n' \neq n_p} \sum_{m' \neq m_p} e^{-i2\pi \frac{q n'}{N}} \\ & \times X_p[n', m'] \beta_j e^{-i2\pi \frac{(k_j + \kappa_j) l_j}{NM}} \\ & \times e^{-i2\pi \left(\frac{k(n' - n_p) - k_j n'}{N} - \frac{(m' - m_p) l - m' l_j}{M} \right)}. \end{aligned} \quad (38)$$

The DFT approach of Section IV can still be used to obtain coarse estimates $(\hat{\theta}_j, \hat{\varphi}_j, \hat{\tau}_j, \hat{\nu}_j)$. Subsequently, an SSR problem can be formulated along the lines of Eq. (28), where the basis matrix Φ_p has its (n_c, j) -th element given as in Eq. (29) except that ξ_j is replaced by $\xi'_j[n_p]$. The presence of $\xi'_j[n_p]$ requires discretization of the fractional number, *i.e.*, $[-0.5 : 0.1 : 0.5]$ given that $\kappa_j \in [-0.5, 0.5]$. The presence of n_p in Eq. (37) suggests that the position of private bins will affect the performance of the SSR estimation. Optimal positioning of private bins will be investigated in future studies. Upon solving the SSR problem, the refined estimates of $(\theta_j, \varphi_j, \tau_j, \nu_j)$ and the channel attenuation factor β_j can be obtained. Substituting these refined estimates into Eq. (11) provides an accurate CSI for the symbol detection.

VII. RECOVERING THE COMMUNICATION INFORMATION

The CSI can be obtained using Eqs. (9) and (10) with estimated $(\theta_j, \varphi_j, \tau_j, \nu_j)$ and β_j . The received time-domain signal is first demodulated into the DD domain, as described in Section II. After performing the equalization, the estimated $\hat{\mathbf{x}}_{n_t}$ can be obtained. Then, the estimated TF domain symbol $\hat{\mathbf{X}}_{n_t}$ can be obtained via ISFFT.

The SFFT (Eq. (6)), which transforms the TF domain symbols into the DD domain, can be expressed as [30]

$$\hat{\mathbf{x}}_{n_t} = \mathbf{G}^{-1} \hat{\mathbf{X}}_{n_t}, \quad (39)$$

where $\hat{\mathbf{X}}_{n_t}$ has $\hat{X}_{n_t}[n, m]$ in its $(m + nM)$ -th position; $\hat{\mathbf{x}}_{n_t}$ has $\hat{x}_{n_t}[k, l]$ in its $(l + kM)$ -th position; and $\mathbf{G} = \mathbf{F}_N^H \otimes \mathbf{F}_M$ is the ISFFT matrix with \mathbf{F}_M being the M -points DFT matrix.

Excluding the pilot bins and guard bins, the TF-DD relations of the p -th antenna can be expressed as

$$\tilde{\mathbf{x}}_p = \tilde{\mathbf{G}}_p^{-1} \tilde{\mathbf{X}}_p, \quad (40)$$

where $\tilde{\mathbf{X}}_p$ is constructed from $\hat{\mathbf{X}}_p$ by excluding the TF pilot/guard bins; $\tilde{\mathbf{x}}_p$ is constructed from $\hat{\mathbf{x}}_p$ by excluding the DD guard bins; and $\tilde{\mathbf{G}}_p$ is constructed based on \mathbf{G} , by removing its row corresponding to TF pilot/guard bins and its column corresponding to DD guard bins. In [34], $\tilde{\mathbf{G}}_p^{-1}$ was referred to as the modified SFFT corresponding to the p -th antenna. The modified SFFT requires knowledge of the locations of the TF pilots/guard bins and the DD guard bins. With the modified SFFT, we can recover the transmitted symbols.

Table I
SYSTEM PARAMETERS

Symbol	Parameter	High-Frequency	Standard
f_c	Carrier frequency	24.25GHz	4GHz
Δf	Subcarrier spacing	120KHz	40KHz
M	# of subcarriers	2048	512
N	# of subsymbols	64	128
$R_{\text{res}} = c\Delta\tau$	Range resolution	1.22m	14.64m
$v_{\text{res}} = \lambda\Delta\nu$	Velocity resolution	23.18m/s	23.42m/s

Table II
CHANNEL PARAMETERS

j	Coordinates	θ_j°	φ_j°	$l_j = l_{cj} + l_{jt}$	$k_j + \kappa_j$
High-Frequency System					
1	(40.5, -13.5)	-12.7	-18.4	85 = 50 + 35	-9 - 0.5
2	(39.4, 28.8)	25.4	36.2	95 = 55 + 40	8 + 0.4
3	(38.3, 39.3)	32.5	45.8	105 = 60 + 45	5 + 0.2
Standard System					
1	(32.9, -29.1)	-23.5	-41.6	8 = 5 + 3	-9 - 0.5
2	(14.6, 56.7)	33.6	75.5	10 = 7 + 4	8 + 0.4
3	(50.0, 69.0)	55.3	55.3	12 = 6 + 6	5 + 0.2

VIII. PILOT OVERHEAD vs SSR COMPLEXITY TRADE-OFF

The overhead of prior methods that use non-overlapped DD pilot designs [8]-[17] is $\eta = N_t[(N_t + 1)l_{\tau_{\max}} + N_t][4k_{\nu_{\max}} + 1]/(N_t NM)$, which depends on the number of transmit antennas N_t . This dependence limits the scalability of those methods to large arrays. This overhead is also subject to the maximum Doppler and delays. As such prior information is not readily available, a larger guard region would need to be used, further increasing the overhead.

For prior methods that use overlapped DD pilots with shared regions [18]-[21], the overhead is reduced to $\eta = N_t[2l_{\tau_{\max}} + 1][4k_{\nu_{\max}} + 1]/(N_t NM)$, which does not depend on N_t after simplification. However, the overhead still depends on the Doppler and delays. Additionally, the underlying algorithm, Sparse Bayesian Learning (SBL), requires a large number of pilots to achieve accurate estimation results. With the increasing number of pilots, the SBL becomes too slow to be practical.

Our proposed method reduces the number of information-bearing symbols by N_t for each TF pilot, resulting in a total pilot overhead of $\eta = N_t N_p / (N_t NM)$, where $N_p \approx P_\tau + P_\nu$. This overhead is independent of the number of transmit antennas, ensuring scalability for large MIMO arrays. Unlike existing methods ([8]-[17]), our overhead doesn't depend on channel parameters, thereby avoiding the need for prior channel information and further reducing overhead. Our design achieves orthogonality at the receiver, facilitating accurate sensing with a minimal number of pilots. Furthermore, increasing N_p enhances the resolution of coarse estimates by refining the discretization of the parameter space. This serves to reduce, rather than increase, the overall complexity.

IX. SIMULATION RESULTS

In this section, we present simulation results to demonstrate the performance of the proposed system. We construct two systems, a *High-Frequency* system with parameters complying

with the 5G NR high frequency protocol [39], and a *Standard* one with parameters complying with the 5G NR standard protocol [39]. The system parameters are shown in Table I. The High-Frequency system delivers a 50% higher data rate than the Standard system, along with a higher range resolution. However, this advantage comes at a cost: its wavelength is one-sixth that of the Standard system, so Doppler shifts are six times larger.

As shown in Table I, the High-Frequency system has a delay resolution of 1.22m, meaning that the scatterer delays will fall on the delay grid. However, for the Standard system, this advantage quickly vanishes. Neither system has a good velocity resolution, resulting in fractional Doppler. The antenna spacing is set to 0.5λ . Unless specified, the constellation is QPSK, the number of transmit antennas is $N_t = 4$, and the pilot power is scaled to the symbol power.

The path scatterers are simulated to lie on a 2D plane. The transmitter is located at $(0, 0)$, and the communication receiver is at $(100, 0)$, *i.e.*, $R_{\text{LoS}} = 100\text{m}$. The coordinates of the J scatterers are listed in Table II, based on which their corresponding AoA θ_j , AoD φ_j , and delay index l_j can be derived (they are also given in the table). The velocities of the scatterers range from 60m/s to 105m/s [40] relative to the communication receiver, directed along θ_j . The corresponding Doppler indices are shown in Table II. The β_j s are generated from a unit power complex Gaussian distribution.

The channel estimation performance is evaluated in terms of the normalized mean square error (NMSE) in [dB]

$$\text{NMSE} = 10 \log_{10} \frac{\|\hat{\mathbf{h}}_{\text{MIMO}} - \mathbf{h}_{\text{MIMO}}\|_{\text{F}}^2}{\|\mathbf{h}_{\text{MIMO}}\|_{\text{F}}^2}, \quad (41)$$

where $\hat{\mathbf{h}}_{\text{MIMO}} \in \mathbb{C}^{N_c NM \times N_t NM}$, is the estimated CSI, obtained based on Eq. (11) using the estimated values of β_j and $(\theta_j, \varphi_j, \tau_j, \nu_j)$; \mathbf{h}_{MIMO} is the true CSI, again obtained based on Eq. (11) using the true value of those parameters; and $\|\cdot\|_{\text{F}}$ is the Frobenius norm. For this analysis, we define a pure Signal-to-Noise Ratio (SNR) to isolate the effect of noise, rather than a Signal-to-Interference-plus-Noise-Ratio (SINR). Although the interference $I_{n,c}[n, m]$ is relevant (*i.e.*, for channel estimation), it is excluded from this specific metric. The SNR is defined as:

$$\text{SNR} \triangleq \frac{P_{\text{Signal}}}{P_{\text{Noise}}} = \frac{\mathbb{E}[\|\mathbf{h}_{\text{MIMO}} \mathbf{x}_{\text{MIMO}}\|^2]}{N_0},$$

where P_{Signal} is the average received signal power and $P_{\text{Noise}} = N_0$ is the average power of the additive white noise. The default SNR is 20dB.

During simulation, each transmit antenna multiplexes information-bearing symbols on the DD grid, leaving N_p randomly selected DD guard bins empty. After converting the DD domain symbols into the TF domain, the pilots and TF guard bins are injected as described in Section III. The frequency arm is located on the TX₁ with support set $\mathcal{P}_1(1, M/2 - P_\tau; P_\tau, P_\nu)$, while the time arm is located on TX₃ with support set $\mathcal{P}_3(N/2 - P_\nu/2, M/2; P_\tau, P_\nu)$. The modulated time-domain signal is constructed as explained in Section II and transmitted. Coarse channel parameter estimates are obtained as described in Section IV. Then, a virtual array is

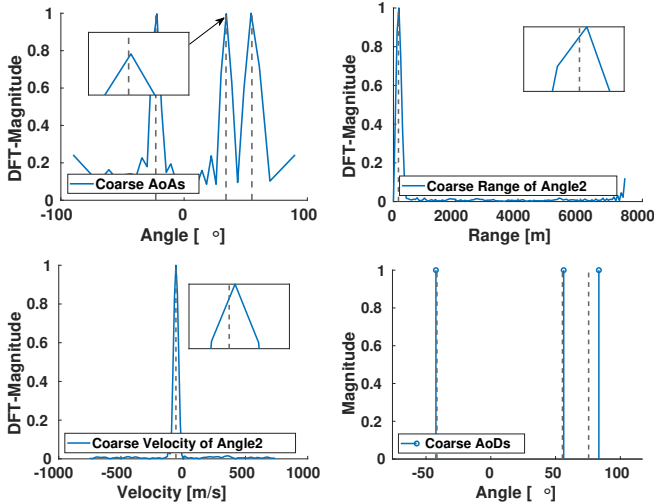


Fig. 5. Coarse estimation in a 4×16 High-Frequency system with $P_\tau = P_\nu = 64$. Due to the limited resolution, visible estimation error is present in coarse estimates. Still, this constrains the parameter space to be discretized, helping the subsequent SSR problem refine the estimates.

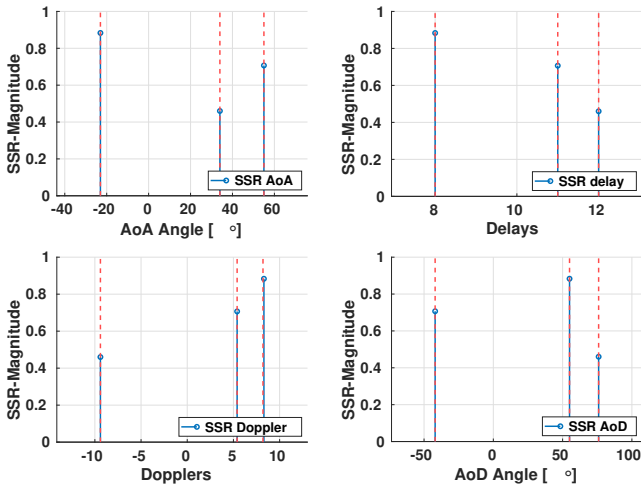


Fig. 6. SSR Estimation. The refined estimates mostly fall on the ground truth, with only a small error shown in Doppler estimates.

constructed as described in Section V based on the orthogonal received TF pilots. An SSR problem is formulated with the dictionary matrix compactly constructed around the coarse estimates. The number of grid points for each scatterer is $G_\theta = 3$, $G_\varphi = 17$, $G_\nu = 5$, and $G_\tau = 11$. There are three scatterers in the channel, and their discretized parameter space may overlap with each other, resulting in a total length of discretized parameter space 7,317, which is the number of columns of $\tilde{\Phi}$. The number of rows is $N_p \times N_c$, e.g., 2,032 for $P_\tau = P_\nu = 64$ and $N_c = 16$. The $\tilde{\Phi}$ is ‘ill-posed’ but is resolvable, attributed to the key property of the SSR technique, which can recover sparse signals from much fewer observations. For the integer Doppler case, the elements in $\tilde{\Phi}$ are taken as in Section V, while for the fractional Doppler case are taken as in Section VI. Upon solving the SSR problem, we obtain the refined estimates.

A. Illustration of Coarse and SSR Estimation

We first illustrate the coarse estimation results described in Section IV. A 4×16 Standard system with $P_\tau = P_\nu = 64$ and the fractional Doppler channel is considered. As can be seen in Fig. 5, due to the limited receive array aperture and limited resolution imposed by P_τ and P_ν , the coarse AoA, range, and velocity estimates corresponding to the second target show visible error. Consequently, the coarse AoD estimates are also limited. Nevertheless, although the coarse estimates exhibit limited accuracy, they define a compact parameter space for solving the subsequent SSR problem. Without coarse estimates, the $\tilde{\Phi}$ matrix would have to be based on a discretization of the entire parameter space, either with a fixed number of $(G_\theta, G_\varphi, G_\nu, G_\tau)$, failing to achieve a fine-grained result, or with an overwhelming large number of discretized points, making the SSR problem unmanageable. The SSR results, obtained as described in Section VI (due to fractional Doppler), are shown in Fig. 6. As can be seen, the parameter estimation is significantly refined, with AoAs, delays, and AoDs aligning with the ground truth, and Dopplers showing a minor error.

B. NMSE Performance

Next, we evaluate the NMSE performance for setups corresponding to various types of Doppler, different SNRs, the number of receive antennas, and the number of pilots. For each setup, we perform 100 Monte Carlo simulations and evaluate the NMSE performance. The average NMSE performance for integer Doppler, i.e., setting $\kappa_j = 0$ of Table II, is shown in Fig. 7. The shaded region represents the standard deviation of the NMSE. Based on Fig. 7, when $\text{SNR} > -6[\text{dB}]$, the High-Frequency system can achieve approximately 2[dB] lower NMSE than the Standard system. This is because the High-Frequency system has a finer range resolution, which helps the SSR distinguish between scatterers that are close in terms of their delay. We also observe that, for the same N_c , increasing the number of pilots does not provide an obvious NMSE improvement. In contrast, for the same pilot overhead, increasing the number of receive antennas from $N_t = 8$ to $N_t = 16$ provides a substantial benefit: the $N_t = 16$ configuration reaches the same NMSE level as the $N_t = 8$ configuration but with an approximately 4[dB] lower SNR requirement ($-12[\text{dB}]$ vs. $-8[\text{dB}]$). This is because with a larger N_c , the coarse AoA estimates benefit from a larger aperture and propagate less error to the consecutive coarse estimates.

For comparison, in Fig. 7 we also evaluate the DD embedded pilot scheme with non-overlapping guard regions [17]. Based on the overhead analysis of Section VIII, each guard region along the Doppler axis requires a width of $4k_{\nu_{\max}} + 1 = 4 \times 9 + 1 = 37$. Therefore, for the case of $N_t = 4$, the grid size for [17] must be $N \geq 4 \times 37 = 148$, which is larger than the values $N = 64$ or $N = 128$ used in our simulations. Thus, our channel configuration does not provide sufficient space for guard regions along the Doppler axis, disadvantaging the method of [17]. As a result, the performance of [17] at low SNR shows significantly higher NMSE as compared to the proposed method. The embedded-pilot method shows a very

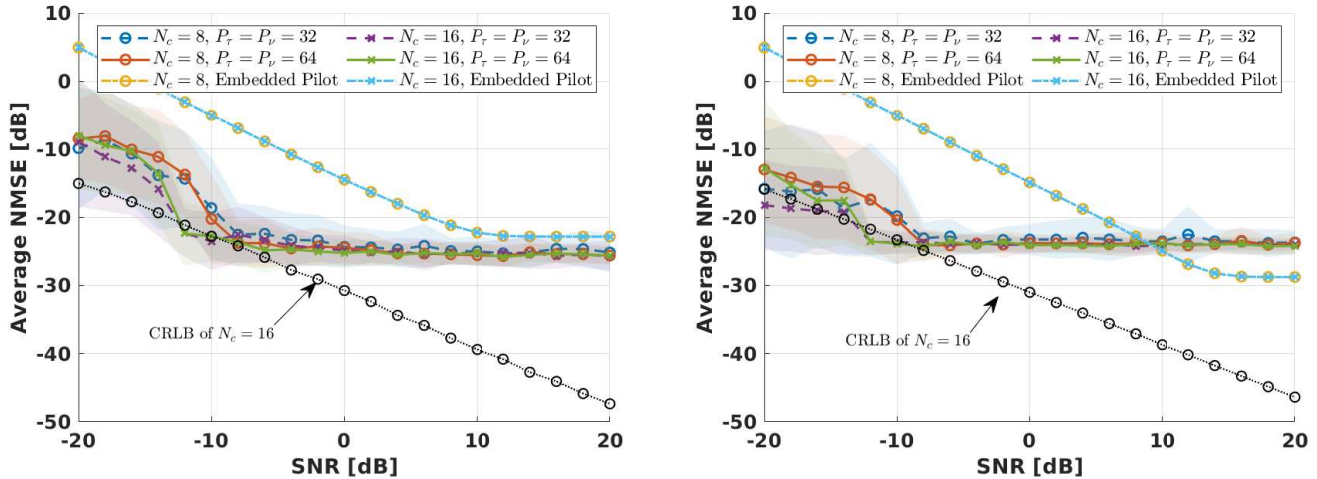


Fig. 7. Average NMSE Performance for Integer Doppler. (Left) High-Frequency System, (Right) Standard System.

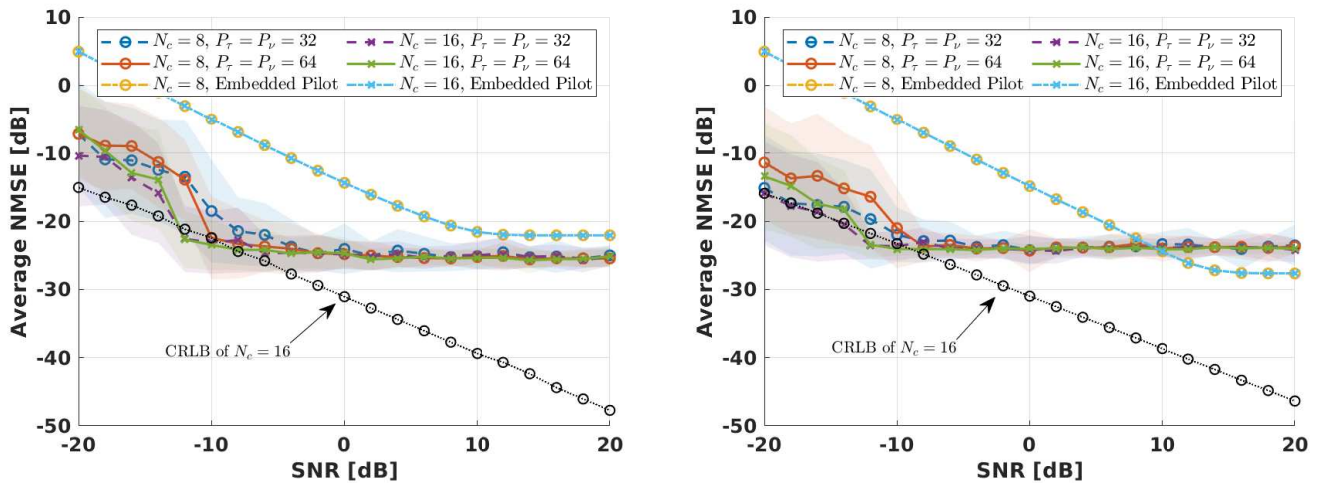


Fig. 8. Average NMSE Performance for Fractional Doppler. (Left) High-Frequency System, (Right) Standard System.

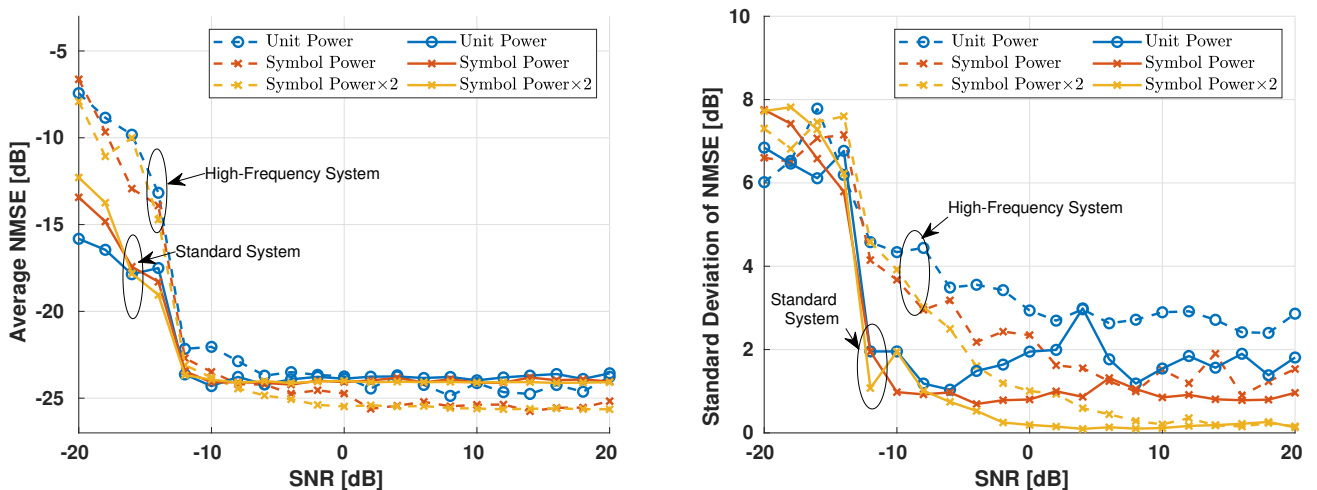


Fig. 9. NMSE Performance with Different Pilot Powers. (Left) Mean, (Right) Standard Deviation.

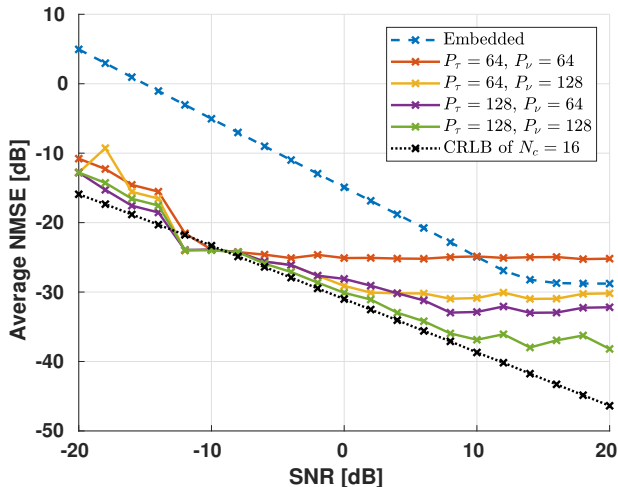


Fig. 10. NMSE Performance of 4×16 Standard System with various N_p .

small standard deviation; however, it suffers from significant NMSE degradation in the High-frequency system, performing worse than the proposed method at all SNR levels. In the Standard system, the embedded pilot method shows a slightly better performance at $\text{SNR} > 8[\text{dB}]$.

We also evaluate the channel with fractional Doppler, as shown in Fig. 8. The NMSE performance is almost identical to the integer Doppler case, demonstrating that the proposed system can effectively handle fractional Doppler.

As a benchmark, the Cramér-Rao Lower Bound (CRLB) for OTFS channel estimation [41] with a single cyclic prefix and a 4×16 MIMO system was calculated and displayed in Figs. 7 and 8. In both systems, the proposed system achieved NMSE performance beyond the CRLB when $N_c = 16$, and attains the CRLB when $N_c = 8$, at $\text{SNR} \in [-14, -10]$ dB, as the constructed virtual array has a larger aperture than the physical array [34]. For comparison, the embedded pilot method follows the slope of the CRLB but never reaches the CRLB at any SNR in either system.

C. Effect of Pilot Power

Next, we investigate the impact of pilot power scaling on NMSE performance. We consider the 4×16 MIMO configuration with $P_\tau = P_\nu = 64$ and the channel with fractional Doppler shifts. The pilot power either remains unit power or scales to either the symbol power or twice the symbol power. The average NMSE performance varies negligibly with pilot power scaling as shown in the left of Fig. 9. However, the standard deviation NMSE performance decreases as the pilot power increases, particularly at high SNR, shown in the right of Fig. 9. Therefore, increasing the pilot power improves the consistency of the channel estimation. This reduction in variation would enhance the long-term stability of the system.

D. Effect of Number of Pilots

The number of pilots (N_p) directly impacts the estimation quality when solving the SSR (Eq. (32)). In Figs. 7 and 8, we

observed that increasing P_τ and P_ν from 32 to 64 offers no significant NMSE improvement. To investigate this, we next test a further increase from 64 to 128, using the 4×16 Standard System with integer Doppler setup and 100 Monte Carlo trials. The results, shown in Fig. 10, demonstrate that this increase from 64 to 128 does reduce the NMSE. Notably, increasing P_τ (frequency) is more effective, providing a 2[dB] NMSE advantage over increasing P_ν (time). This disparity arises because the original 64-point *frequency arm* was the primary bottleneck, exploring only 12.5% (64/512) of the bandwidth. In contrast, the 64-point *time arm* used 50% (64/128) of the subsymbols, offering less room for relative improvement. We also observe that increasing the number of pilots can reduce the NMSE below that of the embedded pilot with the non-overlapped guard region method [17] at high SNR.

E. BER Performance

Here we evaluate the Bit Error Rate (BER) performance of our proposed channel estimation method in a 4×16 MIMO system with fractional Doppler shifts. Various pilot numbers, constellations, and SNRs are considered, and the results are compared with the DD embedded pilot scheme in [17]. For LMMSE equalization, we utilize Matlab's least-squares with QR factorization (LSQR) solver to handle the inversion of the large, sparse channel matrix \mathbf{h}_{MIMO} . As shown in Fig. 11, the CSI obtained from our proposed method effectively recovers the transmitted symbols in both High-Frequency and Standard systems. The method from [17] performs well in High-Frequency systems but exhibits a slightly higher error for high-order modulations and experiences noticeable degradation in the Standard system, which is rooted in pilot-symbol interference. We also find that the High-Frequency system exhibits a slightly faster decrease in BER with increasing SNR compared to the Standard system.

F. Overhead Comparison

We show the overhead of the proposed pilot placement scheme compared to the existing methods [8]-[21] in Fig. 12. The pilot placement of [8]-[17], referred to here as *non-overlapped*, uses guard regions on each transmit antenna, and those guard regions across antennas cannot overlap. The pilot placement of [18]-[21], referred to here as *overlapped*, also requires guard regions; however, multiple antennas share a single guard region. The overhead is calculated as described in Section VIII with the parameters of Tables I and II. We should note that this prior channel information is generally unavailable, leading to higher overhead in practice. The overhead of the non-overlapped pilot design depends on N_t as detailed in Section VIII, while the overhead of the overlapped DD pilot placement does not depend on N_t . However, none of the designs can avoid the overhead increase in the 5G NR High-Frequency system. This is because at high frequencies, the Doppler is more significant, resulting in a larger guard region along the Doppler axis. The 5G NR HF channel also features a wider subcarrier spacing with shorter OTFS symbol duration, leading to a larger guard region along the delay axis. On the contrary, our proposed TF pilot placement is

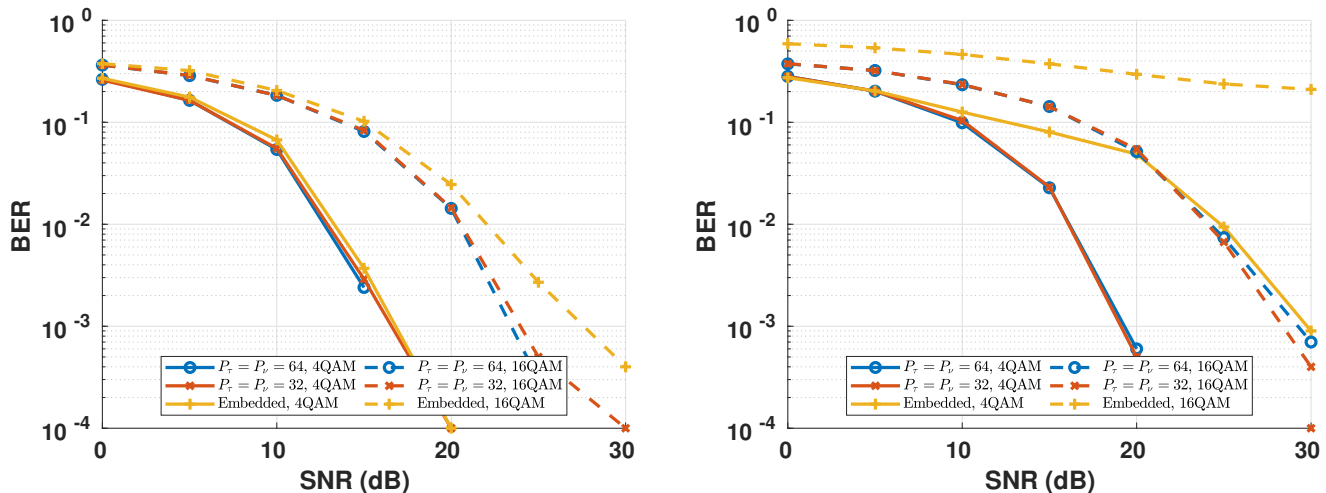


Fig. 11. BER Performance. (Left) High-Frequency System, (Right) Standard System.

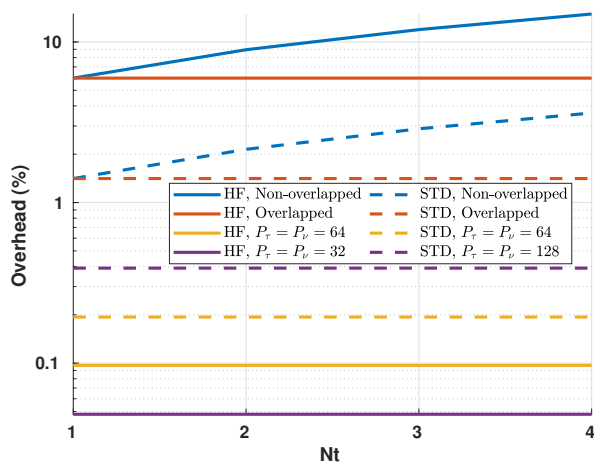


Fig. 12. Overhead of High-Frequency (HF) and Standard (STD) System.

independent of the number of transmit antennas, N_t , as well as the system protocol, making it a promising candidate for wireless systems operated at high frequencies. Approximately, the proposed system's overhead is less than 10% of that of state-of-the-art methods

X. CONCLUSION

We have proposed a novel pilot-aided channel estimation method for MIMO OTFS systems, which features low overhead and good scalability for large MIMO arrays. The pilots are placed on TF domain bins with a dedicated pattern. The TF and DD guard bins are created to ensure the orthogonality of TF pilot bins and the integrity of DD data symbols. The channel estimation is acquired from the received TF pilot bins by first coarsely estimating its parameters using a low-complexity algorithm. Those estimates are then refined by creating a virtual array based on the pilots at the receiver, and formulating and solving an SSR problem, in which the coarse estimates are used to build a low-dimensionality dictionary

matrix. The orthogonal TF pilot bins enable the formation of a virtual array, which improves sensing performance at the cost of some reduction in the DD domain symbols, representing overhead. A small overhead is adequate to acquire high-quality CSI. The proposed system's overhead is independent of the number of transmit antennas, which is preferred in large MIMO systems.

REFERENCES

- [1] W. Saad, M. Bennis, and M. Chen, "A Vision of 6G Wireless Systems: Applications, Trends, Technologies, and Open Research Problems," *IEEE Network*, vol. 34, no. 3, pp. 134–142, 2020.
- [2] S. B. Weinstein, "The History of Orthogonal Frequency-Division Multiplexing," *IEEE Communications Magazine*, vol. 47, no. 11, pp. 26–35, 2009.
- [3] Z. Tao and A. Petropulu, "On the Security of Directional Modulation via Time Modulated Arrays Using OFDM Waveforms," 2025. [Online]. Available: <https://arxiv.org/abs/2408.10522>
- [4] R. Hadani, S. Rakib, M. Tsatsanis, A. Monk, A. J. Goldsmith, A. F. Molisch, and R. Calderbank, "Orthogonal Time Frequency Space Modulation," in *2017 IEEE Wireless Communications and Networking Conference (WCNC)*. San Francisco, CA, USA: IEEE, Mar. 2017, pp. 1–6.
- [5] P. Raviteja, K. T. Phan, Y. Hong, and E. Viterbo, "Interference Cancellation and Iterative Detection for Orthogonal Time Frequency Space Modulation," *IEEE Transactions on Wireless Communications*, vol. 17, no. 10, pp. 6501–6515, Oct. 2018.
- [6] T. Marzetta, E. Larsson, H. Yang, and H. Ngo, *Fundamentals of Massive MIMO*. Cambridge University Press, 2016. [Online]. Available: <https://books.google.com/books?id=IM0iDQAAQBAJ>
- [7] S. Sun, A. P. Petropulu, and H. V. Poor, "MIMO Radar for Advanced Driver-Assistance Systems and Autonomous Driving: Advantages and Challenges," *IEEE Signal Processing Magazine*, vol. 37, no. 4, pp. 98–117, 2020.
- [8] P. Raviteja, K. T. Phan, and Y. Hong, "Embedded Pilot-Aided Channel Estimation for OTFS in Delay-Doppler Channels," *IEEE Transactions on Vehicular Technology*, vol. 68, no. 5, pp. 4906–4917, May 2019.
- [9] Z. Wei, W. Yuan, S. Li, J. Yuan, and D. W. K. Ng, "Off-Grid Channel Estimation With Sparse Bayesian Learning for OTFS Systems," *IEEE Transactions on Wireless Communications*, vol. 21, no. 9, pp. 7407–7426, Sep. 2022.
- [10] M. Tang, H. Wang, Z. Yuan, and J. Yuan, "A Novel Off-Grid Channel Estimation With Fast BCS Using LSM Prior for OTFS Modulation," *IEEE Transactions on Wireless Communications*, vol. 23, no. 9, pp. 12 157–12 171, Sep. 2024.
- [11] Q. Guo, H. Jiang, J. Xiang, and Y. Zhong, "Low Complexity Iterative Channel Estimation and Detection Based on Pilot-Assisted for ZP-OTFS," *IEEE Communications Letters*, vol. 29, no. 4, pp. 724–728, Apr. 2025.

- [12] P. Sun, M. Dong, Q. Guo, J. Cui, H. Yu, and F. Liu, "Low Complexity Channel Estimation Based on UAMP for Orthogonal Time Frequency Space Systems," *IEEE Communications Letters*, vol. 29, no. 10, pp. 2208–2212, Oct. 2025.
- [13] H.-G. Lee, J. Kim, J. Zhao, and J. Joung, "Single-Tone-Based Channel Estimation Method for OTFS Systems," *IEEE Transactions on Communications*, vol. 73, no. 3, pp. 1638–1651, Mar. 2025.
- [14] Q. Wang, X. Chen, Q. Tao, L. P. Qian, P.-Y. Kam, and Y. Wu, "Model-Driven Channel Estimation Network for Orthogonal Time-Frequency Space Systems," *IEEE Transactions on Vehicular Technology*, vol. 74, no. 7, pp. 11 552–11 556, Jul. 2025.
- [15] X. Li, Y. Liang, Z. Zhou, and P. Fan, "Fractional Delay-Doppler Channel Estimation for OTFS Systems Based on Segmentation Technique and Sparse Bayesian Learning," *IEEE Communications Letters*, vol. 29, no. 5, pp. 1067–1071, May 2025.
- [16] H. Zhang, X. Huang, and J. A. Zhang, "Low-Overhead OTFS Transmission With Frequency or Time Domain Channel Estimation," *IEEE Transactions on Vehicular Technology*, vol. 73, no. 1, pp. 799–811, Jan. 2024.
- [17] M. Kollengode Ramachandran and A. Chockalingam, "MIMO-OTFS in High-Doppler Fading Channels: Signal Detection and Channel Estimation," in *2018 IEEE Global Communications Conference (GLOBECOM)*, Abu Dhabi, United Arab Emirates: IEEE, Dec. 2018, pp. 206–212.
- [18] W. Shen, L. Dai, J. An, P. Fan, and R. W. Heath, "Channel Estimation for Orthogonal Time Frequency Space (OTFS) Massive MIMO," *IEEE Transactions on Signal Processing*, vol. 67, no. 16, pp. 4204–4217, Aug. 2019.
- [19] H. Wang, Q. Chen, X. Wang, W. Du, X. Li, and A. Nallanathan, "Adaptive Block Sparse Backtracking-Based Channel Estimation for Massive MIMO-OTFS Systems," *IEEE Internet of Things Journal*, vol. 12, no. 1, pp. 673–682, Jan. 2025.
- [20] D. Shi, W. Wang, L. You, X. Song, Y. Hong, X. Gao, and G. Fettweis, "Deterministic Pilot Design and Channel Estimation for Downlink Massive MIMO-OTFS Systems in Presence of the Fractional Doppler," *IEEE Transactions on Wireless Communications*, vol. 20, no. 11, pp. 7151–7165, Nov. 2021.
- [21] L. Zhao, J. Yang, Y. Liu, and W. Guo, "Block Sparse Bayesian Learning-Based Channel Estimation for MIMO-OTFS Systems," *IEEE Communications Letters*, vol. 26, no. 4, pp. 892–896, Apr. 2022.
- [22] W. Yuan, S. Li, Z. Wei, J. Yuan, and D. W. K. Ng, "Data-Aided Channel Estimation for OTFS Systems With a Superimposed Pilot and Data Transmission Scheme," *IEEE Wireless Communications Letters*, vol. 10, no. 9, pp. 1954–1958, 2021.
- [23] H. B. Mishra, P. Singh, A. K. Prasad, and R. Budhiraja, "OTFS Channel Estimation and Data Detection Designs With Superimposed Pilots," *IEEE Transactions on Wireless Communications*, vol. 21, no. 4, pp. 2258–2274, 2022.
- [24] M. A. Sheikh, A. Rajoriya, P. Singh, and R. Budhiraja, "Bayesian Learning-Aided Channel Estimators for Superimposed-Pilot-Based OTFS Systems," *IEEE Transactions on Communications*, vol. 73, no. 2, pp. 950–967, Feb. 2025.
- [25] Y. Liu, Y. L. Guan, and D. González G., "BEM OTFS Receiver with Superimposed Pilots over Channels with Doppler and Delay Spread," in *ICC 2022 - IEEE International Conference on Communications*, 2022, pp. 2411–2416.
- [26] F. Huang, Q. Guo, Y. Zhang, and Y. V. Zakharov, "Message Passing-Based Joint Channel Estimation and Signal Detection for OTFS With Superimposed Pilots," *IEEE Transactions on Vehicular Technology*, vol. 73, no. 8, pp. 11 531–11 542, 2024.
- [27] H.-T. Sheng and W.-R. Wu, "Time-Frequency Domain Channel Estimation for OTFS Systems," *IEEE Transactions on Wireless Communications*, vol. 23, no. 2, pp. 937–948, Feb. 2024.
- [28] A. Mehrotra, S. Srivastava, A. K. Jagannatham, and L. Hanzo, "Data-Aided CSI Estimation Using Affine-Pre-coded Superimposed Pilots in Orthogonal Time Frequency Space Modulated MIMO Systems," *IEEE Transactions on Communications*, vol. 71, no. 8, pp. 4482–4498, 2023.
- [29] S. Srivastava, R. K. Singh, A. K. Jagannatham, and L. Hanzo, "Bayesian Learning Aided Sparse Channel Estimation for Orthogonal Time Frequency Space Modulated Systems," *IEEE Transactions on Vehicular Technology*, vol. 70, no. 8, pp. 8343–8348, Aug. 2021.
- [30] —, "Delay-Doppler and Angular Domain 4D-Sparse CSI Estimation in OTFS Aided MIMO Systems," *IEEE Transactions on Vehicular Technology*, vol. 71, no. 12, pp. 13 447–13 452, Dec. 2022.
- [31] —, "Bayesian Learning Aided Simultaneous Row and Group Sparse Channel Estimation in Orthogonal Time Frequency Space Modulated MIMO Systems," *IEEE Transactions on Communications*, vol. 70, no. 1, pp. 635–648, Jan. 2022.
- [32] A. Mehrotra, S. Srivastava, S. Asifa, A. K. Jagannatham, and L. Hanzo, "Online Bayesian Learning-Aided Sparse CSI Estimation in OTFS Modulated MIMO Systems for Ultra-High-Doppler Scenarios," *IEEE Transactions on Communications*, vol. 72, no. 4, pp. 2182–2200, Apr. 2024.
- [33] C. Chen, J. Zhang, Y. Han, J. Lu, and S. Jin, "Channel Estimation for Massive MIMO-OTFS System in Asymmetrical Architecture," *IEEE Signal Processing Letters*, vol. 30, pp. 1412–1416, 2023.
- [34] K. Wang and A. Petropulu, "ISAC MIMO Systems with OTFS Waveforms and Virtual Arrays," *IEEE Journal on Selected Areas in Communications*, pp. 1–1, 2025.
- [35] —, "A Bandwidth Efficient Dual Function Radar Communication System Based on a MIMO Radar Using OTFS Waveforms," in *ICASSP 2025 - 2025 IEEE International Conference on Acoustics, Speech and Signal Processing (ICASSP)*. Hyderabad, India: IEEE, Apr. 2025, pp. 1–5.
- [36] —, "Virtual Array for Dual Function MIMO Radar Communication Systems using OTFS Waveforms," in *2025 IEEE 5th International Symposium on Joint Communications & Sensing (JC&S)*. Oulu, Finland: IEEE, Jan. 2025, pp. 1–6.
- [37] —, "Low Overhead MIMO-OTFS Channel Estimation," accepted by The 33rd European Signal Processing Conference (EUSIPCO 2025).
- [38] F. Gomez-Cuba, "Compressed Sensing Channel Estimation for OTFS Modulation in Non-Integer Delay-Doppler Domain," in *2021 IEEE Global Communications Conference (GLOBECOM)*. Madrid, Spain: IEEE, Dec. 2021, pp. 1–6.
- [39] W. Vook, A. Ghosh, E. Diarte, and M. Murphy, "5G New Radio: Overview and Performance," in *2018 52nd Asilomar Conference on Signals, Systems, and Computers*, 2018, pp. 1247–1251.
- [40] "Minimum Requirements Related to Technical Performance for IMT-2020 Radio Interface(s)," Jan. 2025, [Online; accessed 21. Jan. 2025]. [Online]. Available: <https://www.itu.int/pub/R-REP-M.2410>
- [41] J. Pan, "Cramer-Rao Low Bound of Channel Estimation for Orthogonal Time Frequency Space Modulation System," *IEEE Transactions on Vehicular Technology*, vol. 70, no. 10, pp. 9646–9658, Oct. 2021.